

pubs.acs.org/JPCA Article

Calculating Reliable Gibbs Free Energies for Formation of Gas-Phase Clusters that Are Critical for Atmospheric Chemistry: (H₂SO₄)₃

Luke A. Kurfman, Tuguldur T. Odbadrakh, and George C. Shields*



Cite This: J. Phys. Chem. A 2021, 125, 3169–3176



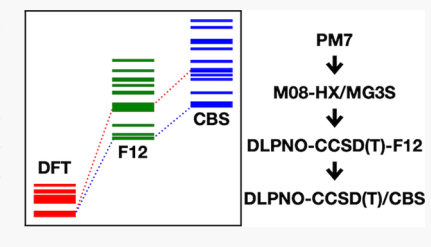
ACCESS

Metrics & More

Article Recommendations

Supporting Information

ABSTRACT: The effects of atmospheric aerosols on our climate are one of the biggest uncertainties in global climate models. Calculating the pathway for the formation of prenucleation clusters that become aerosols is challenging, requiring a comprehensive analysis of configurational space and highly accurate Gibbs free energy calculations. We identified a large set of minimum energy configurations of $(H_2SO_4)_3$ using a sampling technique based on a genetic algorithm and a stepwise density functional theory (DFT) approach and computed the thermodynamics of formation of these configurations with more accurate wavefunction-based electronic energies computed on the DFT geometries. The DLPNO-CCSD(T) methods always return more positive energies compared to the DFT energies.



Within the DLPNO-CCSD(T) methods, extrapolating to the complete basis set limit gives more positive free energies compared to explicitly correlated single-point energies. The CBS extrapolation was shown to be robust as both the 4-5 inverse polynomial and Riemann zeta function schemes were within chemical accuracy of one another.

■ INTRODUCTION

The effects of atmospheric aerosols on our climate are one of the biggest uncertainties in global climate models, thought to be a major contributor to cooling the atmosphere through cloud condensation. Aerosols are defined as gas-phase molecular clusters ranging from approximately 2 nm to 100 μ m in diameter that are suspended in the atmosphere and are necessary for the formation and growth of cloud condensation nuclei (CCN). Aerosols can be formed from the direct emission of natural and human-made gases (primary aerosols) as well as from the processing of these primary species by atmospheric reactions (secondary aerosols). When an aerosol particle reaches its critical size, its growth through the uptake of water and other atmospheric species outpaces its decay through fragmentation and a CCN can be formed, leading to cloud droplets. Arguably, the most important type of aerosol is the sulfuric acid aerosol,² contributing up to 0.4±0.2 W m⁻² toward a cooling effect on the atmosphere through the resulting cloud droplets.3 The primary sources of sulfuric acid aerosols are secondary aerosols, with the burning of fossil fuels and biomass contributing the most to the formation of these secondary aerosols by releasing SO₂ into the atmosphere. Sulfate can then be oxidized by hydroxyl free radicals (OH) to eventually form sulfuric acid.

We have explored the thermodynamics of formation of prenucleation clusters of water, ⁵⁻⁹ sulfuric acid and its dimers, ^{10,11} ammonia and amines, ^{12,13} and other species ¹⁴⁻¹⁶ with a focus on hydrogen bonding interactions. In this paper, we report on our investigation of the thermodynamics of formation of ternary clusters of sulfuric acid. This pursuit requires a thorough exploration of the configurational space of the gas-phase sulfuric acid trimers followed by the calculation

of accurate electronic and vibrational energies. The configurational space of the sulfuric acid trimer is much larger compared to the monomer and dimer, with only a couple of minimum energy structures identified for the monomer¹⁰ and only four low-energy structures identified for the sulfuric acid dimer. 11 Furthermore, the dynamic nature of the atmosphere requires that the thermodynamics of formation of atmospheric clusters be computed for a range of temperatures representing different altitudes, with most studies using 216.65 K to represent the top of the troposphere, 273.15 K for an intermediate layer, and 298.15 K at sea level. Because different global minimum structures exist at different temperatures and are generally different from the electronic minimum, a sufficient number of local minimum structures around the global minimum needs to be retained throughout the procedure. Equally important in retaining a sufficiently large pool of local minimum structures is the accuracy of the final electronic and vibrational energies. To this end, density functional theory (DFT) has proven invaluable as it balances computational cost with accuracy. Various researchers have successfully employed the PW91, B3LYP, 18 and ω B97 19 families of exchange-correlation functionals, usually coupled with large Pople basis sets.²⁰ In particular, the dispersion-corrected ωB97X-D/6-31++G- $(d,p)^{37-41,43-45}$ method has proven robust. In addition, high-

Received: January 30, 2021 Revised: March 15, 2021 Published: April 7, 2021





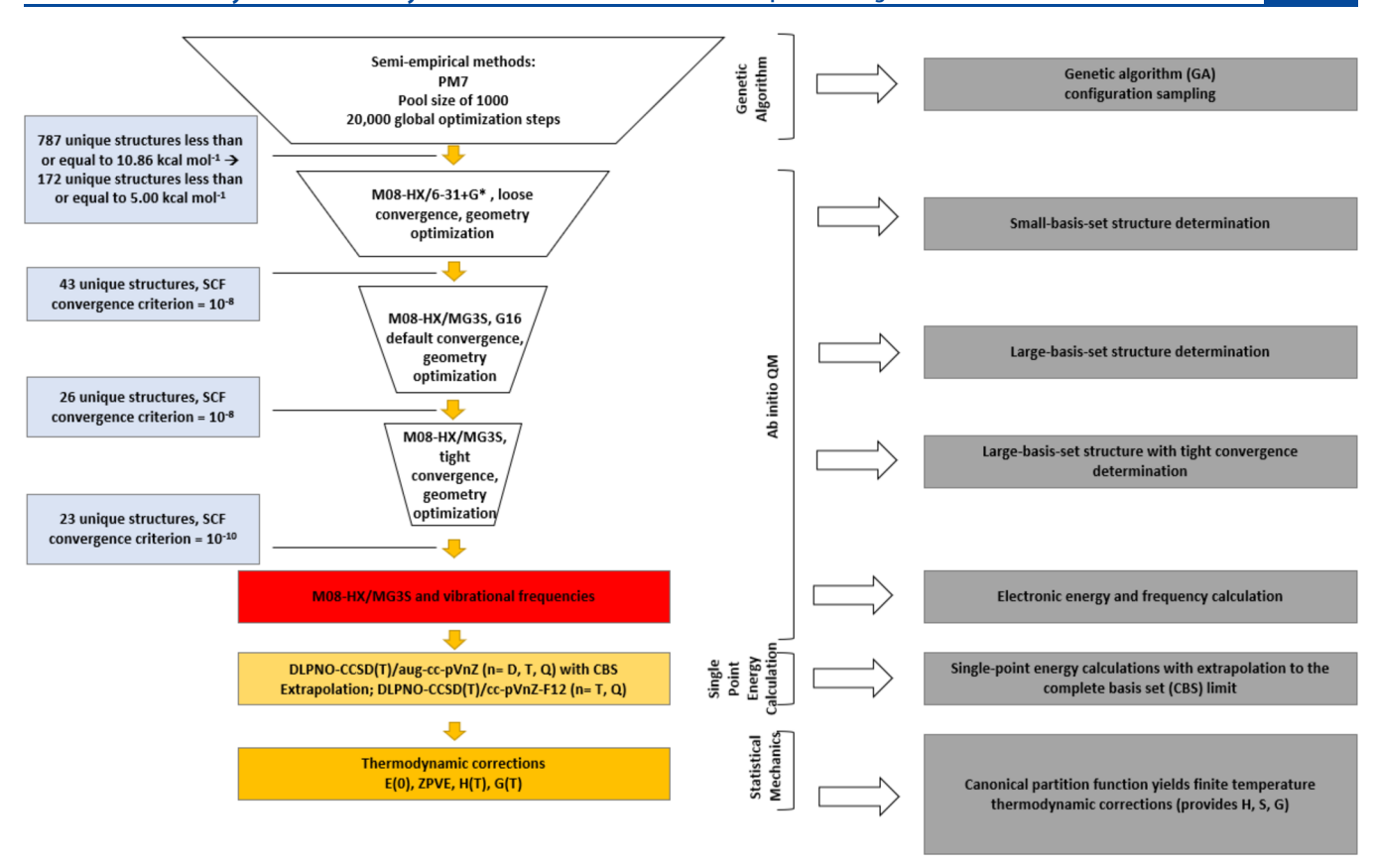


Figure 1. Diagram of the optimization and single-point energy calculation scheme used in this study.

level electronic energies have been used along with the DFT geometries using methods such as the resolution-of-identity second-order Moller–Plesset perturbation theory RI-MP2/aug-cc-pV(T+d)Z with satisfactory results. Recently, the linear-scaling domain-based local pair-natural orbital coupled-cluster method DLPNO-CCSD(T) $^{21-29}$ has opened up the possibility to approach complete basis set limit accuracies at DFT costs.

In computing the thermodynamic corrections using the canonical partition function, the use of harmonic vibrational frequencies presents a source of error due to its poor description of low-frequency modes associated with shallow potentials. A detailed look at small water clusters shows that scaled harmonic frequencies are as good as anharmonic frequencies at predicting all of the frequencies for (H₂O)₂₋₅. Temelso et al. employed scaled harmonic vibrational frequencies to correct for this for sulfuric acidwater clusters by using matching second-order vibrational perturbation theory (VPT2) results. For the hydrated sulfuric acid monomer, the zero-point vibrational energy, Hvib (298.15 K), and Svib (298.15 K) were calculated using the scaling factors of 0.979, 1.077, and 1.102, respectively, resulting in a change of -0.47 kcal mol⁻¹ in the free energy.¹⁰ In another case, scaling factors of 0.981, 1.110, and 1.095 for the sulfuric acid dimer resulted in a change of -0.69 kcal mol⁻¹. Myllys et al. evaluated the effects of frequency scaling versus VPT2 as well as a quasi-harmonic approximation in sulfuric acid-amine clusters and showed that both scaling to match VPT2 and the pure VPT2 frequencies reduce the thermal contribution of vibrations by about 1.6-1.7%, while the quasi-harmonic approximation increases it by up to 7.8%.31 Ultimately, the scaling or exclusion of low-frequency harmonic vibrational

modes seems to have mild effects on the final Gibbs free energy of formation when compared to larger contributions to the canonical partition function.

In the current work, we have investigated the formation of the sulfuric acid trimer using a wide range of electronic structure approaches. To this end, we first identified a large set of minimum energy configurations of $(H_2SO_4)_3$ using a sampling technique based on a genetic algorithm. These structures were then refined using a stepwise DFT approach until a final set of minima was identified at a sufficiently accurate level of theory. Finally, we computed the thermodynamics of formation of these configurations with more accurate wavefunction-based electronic energies computed on the DFT geometries. The electronic energies were computed at various levels of theory, including complete basis set limit (CBS) extrapolations as well as using explicitly correlated methods. We first present our computational methodology and then our results and their consequences.

■ COMPUTATIONAL METHODOLOGY

The identification of low-energy configurations of $(H_2SO_4)_3$ was accomplished by first generating a large set of rough geometries using a genetic algorithm (GA) and then refining those geometries through a number of increasingly accurate DFT geometry optimizations. The initial set of GA geometries was generated using the OGOLEM program³² on the PM7³³ semi-empirical potential energy surface (PES) implemented in MOPAC2016.³⁴ This algorithm takes an initial pool of randomly generated configurations and changes them according to an evolutionary algorithm until a final set of converged structures is found. The initial pool size was chosen to be 1000 configurations, and the process was allowed to run for 20,000

iterations or until convergence. The final set of GA structures was then screened for uniqueness to eliminate double counting by comparing their rotational constants and energies resulting in 787 PM7 minima, with the highest-energy structure existing 10.86 kcal mol⁻¹ above the PM7 minimum. Two structures were deemed identical if their rotational constants and energies are within 1% or 0.1 kcal mol⁻¹ of one another, respectively. These structures were used as inputs in the following DFT geometry optimization steps.

In the first pass, the 172 PM7 structures within 5 kcal mol⁻¹ of the global minimum on the PM7 PES were further optimized at the M08-HX/6-31+G* level of theory 20,35,36 using loose convergence criteria (RMS Force = 0.001667 au, maximum displacement = 0.01 au) in Gaussian 2016 Rev. B.01.37 The converged geometries were then screened for uniqueness using the criteria mentioned above, after which the resulting set of unique geometries was further optimized at the M08-HX/MG3S level of theory, using the Gaussian 16 default convergence criteria (RMS Force = 0.0003 au, maximum displacement = 0.00180). ^{36,38,39} The combination of the M08-HX density functional with the MG3S basis set has been shown to give accurate bond lengths and angles for gas-phase noncovalent molecular clusters.³⁵ Finally, the resulting set of unique geometries was once again optimized at the M08-HX/ MG3S level of theory using tighter convergence criteria (RMS Force = 0.000010 au, maximum displacement = 0.000060 au), and the harmonic vibrational frequencies were calculated on the converged geometries. The harmonic vibrational frequencies were then used to compute thermodynamic corrections to the energy at temperatures of 216.65, 273.15, and 298.15 K and a pressure of 1 atm using a modified version of the THERMO.PL script from the National Institute of Standards and Technology. 40,41 A detailed description of the above protocol can be found in a recent publication.⁴²

The Gibbs free energy of formation of gas-phase clusters is highly sensitive to the electronic structure method because the electronic energy is the largest contribution to the partition function. In order to ensure the accuracy of electronic energies as well as reasonable computational costs, various domain local-pair natural-orbital coupled-cluster methods with single, double, and perturbative triple excitations (DLPNO-CCSD-(T))^{21–29,43–45} were employed along with two different CBS extrapolation schemes. The electronic energies of the final set of low-energy configurations were calculated at the DLPNO-CCSD(T)/aug-cc-pVnZ (n = D, T, Q) level of theory implemented in the ORCA 4.2.1 program, 46,47 and these energies were used in three-point 4-5 inverse polynomial⁴⁸ and Riemann zeta function⁴⁹ CBS extrapolation schemes using inhouse scripts. The CBS expressions for the Riemann zeta function method are given in ref 49, while derivations of the 4-5 inverse polynomial expressions are included in the Supporting Information. Furthermore, explicitly correlated DLPNO-CCSD(T)-F12/cc-pVnZ-F12 (n = T, Q) electronic energies were computed using the resolution-of-identity Coulomb/exchange and CABS density-fitting auxiliary basis sets. 45,50 Finally, these high-level electronic energies were combined with the DFT thermodynamic corrections to compute the Gibbs free energy of formation of (H₂SO₄)₃. The above protocol is represented diagrammatically in Figure 1.

RESULTS AND DISCUSSION

Minimum Energy Structures. We have identified $13 \, (H_2SO_4)_3$ clusters with electronic energies $<2 \, kcal \, mol^{-1}$ of the M08-HX/MG3S global minimum. These clusters exhibit two main structural motifs depending on the hydrogen bonding arrangements: linear and triangular. We found three linear clusters, shown in Figure 2, in which a central sulfuric acid

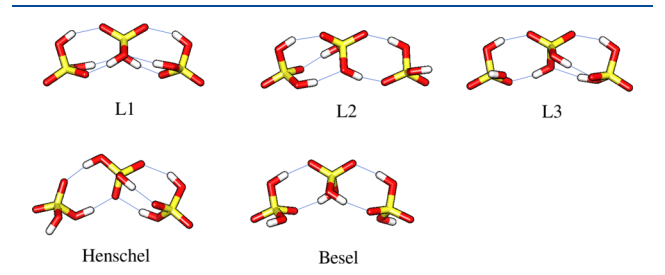


Figure 2. M08-HX/MG3S optimized structures of linear $(H_2SO_4)_3$ clusters. Structures L1–L3 were found using our methodology, whereas Henschel and Besel were extracted from the literature and reoptimized at the M08-HX/MG3S level of theory. Visualization was generated using Chimera UCSF. 54

molecule forms a hydrogen bond bridge between two noninteracting terminal sulfuric acid molecules. Furthermore, we have reoptimized two more linear structures from the existing literature in order to better evaluate the performance of our methodology. In addition, we found 10 triangular clusters, shown in Figure 3, where each sulfuric acid molecule forms at

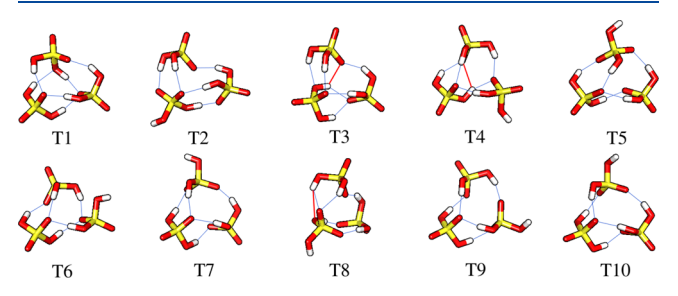


Figure 3. M08-HX/MG3S optimized structures of triangular $(H_2SO_4)_3$ clusters. Close interactions outside our criteria for hydrogen bonds (distances less than 2.4 Å and angles greater than roughly 140°) are colored red. Visualization was generated using Chimera UCSF. ⁵⁴

least one hydrogen bond to the other two sulfuric acid molecules. To our knowledge, most of these triangular clusters have not been described in the literature and are unique to our methodology. The mirror image of L3 has been previously reported by Herb et al., ⁵¹ and the mirror image of T7 was reported by Kubečka et al. ⁵² The mirror image of T1 and T3 are reported by de Souza Gonçalves to be the two lowest electronic energy clusters at the M06-2X/aug-cc-pVTZ level of theory, corresponding to their structures M06-SAT1 and M06-SAT2, respectively. ⁵³

All of the structures presented here except one have five to six true hydrogen bonds, where a hydrogen bond is defined as hydrogen—oxygen distances of less than 2.4 Å and O–H···O bond angles between 140° and 180° . A few hydrogen bonds had bond angles between 135° and 140° but had shorter H–O distances and so were included. The linear Besel structure has only four hydrogen bonds.

Impact of Configurational Sampling Cutoffs in the **PM7 Step.** It has been known for a long time that the PMx methods are much better at predicting hydrogen-bonded structures than they are at predicting accurate energies. 55 As discussed in the methods section and in Figure 1, the genetic algorithm used a cutoff of 5 kcal mol⁻¹ at the PM7 level of theory to produce the final set of 23 M08-HX/MG3S structures. However, structures reported by Henschel et al.⁵⁶ (originally reported by Torpo et al.⁵⁷) and Besel et al.⁵⁸ were not captured within that 5 kcal mol⁻¹ cutoff. A search through all 787 PM7 structures (Figure 1) using ArbAlign⁵⁹ to find structures with low RMSDs relative to the Bessel and Herschel structures revealed that some of the PM7 structures in the 5.75-6.50 kcal mol⁻¹ range did converge to the Besel and Henschel structures after M08-HX/MG3S optimization of these structures. These results show that, to capture all the relevant previously published structures, a minimum cutoff of at least 7-8 kcal mol⁻¹ was necessary. This leads us to conclude that, if PM7 is used as an initial conformational analysis step, the cutoffs must be higher than 5 kcal mol⁻¹, and we recommend at least 7-8 kcal mol⁻¹. In addition, after completing the energetic comparisons with DLPNO-CCSD-(T) methods, we learned that the DFT method bunches the clusters much closer together than the DLPNO-CCSD(T)// DFT energies, which are spread out considerably after these single-point-energy calculations. Furthermore, the entire PES for the PM7 clusters is compressed relative to the M08-HX/6-31+G* PES such that there is no absolute way to identify which of the many PM7 configurations will end up in the final set of M08-HX/MG3S low-energy structures. Figure S1 in the Supporting Information shows the energy distributions of configurations optimized at the PM7 (red), M08-HX/6-31+G* (green), and M08-HX/MG3S (blue and black) steps of our methodology. It is clear that the M08-HX/6-31+G* geometry optimizations spread out the very dense set of PM7 energies. Thus, the only way to ensure that we have identified all of the PM7 structures that will eventually result in our final set of minima is to use a large pool size and run each and every one of the PM7 configurations through the M08-HX/6-31+G*

Electronic Energies. For each cluster shown in Figures 2 and 3, we present the electronic energies of formation computed using eq 1 below

$$\Delta E_{el} = E_{el}[(H_2SO_4)_3] - 3E_{el}[H_2SO_4]$$
 (1)

where $E_{\rm el}[({\rm H_2SO_4})_3]$ is the electronic energy of the sulfuric acid trimer and $E_{\rm el}[{\rm H_2SO_4}]$ is the electronic energy of an isolated sulfuric acid molecule. This equation represents the electronic energy change of the process of forming the bound trimer from infinitely separated monomers in the gas phase at 0 K. Table 1 lists the $\Delta E_{\rm el}$ of the clusters calculated at the M08-HX/MG3S, DLPNO-CCSD(T)-F12/cc-pVTZ-F12, DLPNO-CCSD(T)/CBS(Riemann zeta), and DLPNO-CCSD(T)/CBS(4-5 polynomial) levels of theory. The CBS values are three-point extrapolations using the aug-cc-pVnZ (n = D, T, Q) basis sets, hereafter referred to as aVnZ for brevity.

Table 1 reveals that M08-HX favors the triangular structures while the CCSD(T) methods favor linear structures. Structures with five hydrogen bonds are predicted to be the minima across all methods for Gibbs free energy, while structures with six hydrogen bonds are found as the minima for DFT for electronic energy and enthalpy (273 and 298 K) compared to the DLPNO-CCSD(T) methods. In addition, DFT binds

Table 1. Electronic Formation Energies of (H₂SO₄)₃ Clusters in Units of kcal mol^{-1a}

| cluster | M08- HX/ MG3S | DLPNO- CCSD(T)-F12/ cc-pVTZ-F12 | DLPNO- CCSD(T)/ CBS(Riemann) | DLPNO- CCSD(T) /CBS(4-5) |
|------------------|---------------------|---------------------------------------|------------------------------------|--------------------------------|
| structure T1 | -41.00 | -34.31 | -31.92 | -32.28 |
| structure T2 | -40.21 | -34.11 | -32.13 | -32.42 |
| structure L1 | -40.11 | -34.87 | -33.06 | -33.31 |
| structure T3 | -39.97 | -33.08 | -30.89 | -31.22 |
| structure T4 | -39.79 | -33.42 | -31.41 | -31.71 |
| structure T5 | -39.79 | -33.32 | -31.24 | -31.56 |
| structure T6 | -39.74 | -33.57 | -31.44 | -31.76 |
| structure T7 | -39.55 | -33.81 | -32.13 | -32.40 |
| structure T8 | -39.47 | -32.91 | -31.15 | -31.42 |
| structure T9 | -39.39 | -34.41 | -32.68 | -32.95 |
| structure L2 | -39.34 | -35.25 | -33.43 | -33.67 |
| structure T10 | -39.33 | -34.11 | -32.31 | -32.59 |
| structure L3 | -39.22 | -34.79 | -33.06 | -33.30 |
| Henschel | -38.79 | -34.54 | -32.75 | -32.99 |
| Besel | -37.63 | -33.68 | -31.88 | -32.13 |

"The first column lists the cluster names as presented in Figures 2 and 3. The second column lists the DFT energies calculated at the M08-HX/MG3S level of theory. The third column lists the explicitly correlated energy calculated at the DLPNO-CCSD(T)-F12/cc-pVTZ-F12 level of theory. The fourth and fifth columns list the three-point (aVDZ, aVTZ, and aVQZ) complete basis set limit extrapolation energies calculated using the Riemann zeta and 4-5 inverse polynomial schemes, respectively. For each method, the lowest electronic formation energy is denoted in bold.

much more strongly compared to any of the DLPNO-CCSD(T)//DFT methods. This means that the Gibbs free energies calculated using DFT electronic contributions may lead to overestimation of the formation equilibrium constant by many orders of magnitude because of the equilibrium constant's exponential dependence on Gibbs free energy. In addition, the CBS extrapolated energies using the 4-5 and Riemann methods are extremely close, providing additional confidence in both extrapolation procedures. Comparing the CBS values to the explicitly correlated F12 numbers reveals that the cc-pVTZ-F12 values are generally 2 to 3 kcal mol⁻¹ more negative than the CBS values. To address this point, we calculated the cc-pVQZ-F12 values for three of the structures in Table 1. We found that the DLPNO-CCSD(T)-F12/ccpVQZ-F12 electronic energies for L2, L3, and Henschel structures were -35.65, -35.16, and -34.90 kcal mol⁻¹, which are close to the DLPNO-CCSD(T)-F12/cc-pVTZ-F12 results in Table 1. Thus, the explicitly correlated F12 methods are the same with both the triple zeta and quadruple basis sets. This raises the question of how reliable the explicitly correlated F12 methods will be compared to the traditional CBS extrapolation

Gibbs Free Energies at 298 K by Each Method. Table 2 lists the resulting standard Gibbs free energies (ΔG°) of

Table 2. Gibbs Free Energies of Formation of $(H_2SO_4)_3$ Clusters at a Temperature of 298.15 K in Units of kcal mol^{-1a}

| cluster | M08- HX/ MG3S | DLPNO- CCSD(T)-F12/ cc-pVTZ-F12 | DLPNO- CCSD(T)/ CBS(Riemann) | DLPNO- CCSD(T) /CBS(4-5) |
|------------------|---------------------|---------------------------------------|------------------------------------|--------------------------------|
| structure T1 | -12.18 | -5.48 | -3.09 | -3.45 |
| structure T2 | -13.48 | -7.39 | -5.40 | -5.69 |
| structure L1 | -12.55 | -7.31 | -5.50 | -5.75 |
| structure T3 | -11.80 | -4.91 | -2.72 | -3.04 |
| structure T4 | -12.65 | -6.29 | -4.27 | -4.58 |
| structure T5 | -12.47 | -6.01 | -3.93 | -4.25 |
| structure T6 | -12.10 | -5.93 | -3.80 | -4.12 |
| structure T7 | -12.39 | -6.66 | -4.97 | -5.24 |
| structure T8 | -13.28 | -6.72 | -4.96 | -5.23 |
| structure T9 | -12.66 | -7.67 | -5.95 | -6.22 |
| structure L2 | -13.28 | -9.18 | -7.37 | -7.61 |
| structure T10 | -12.74 | -7.52 | -5.72 | -6.00 |
| structure L3 | -13.42 | -8.99 | -7.25 | -7.49 |
| Henschel | -13.47 | -9.22 | -7.43 | -7.66 |
| Besel | -12.45 | -8.49 | -6.70 | -6.94 |
| arra c | | | 1 | |

^aThe first column lists the cluster names as presented in Figures 2 and 3. Then each column thereafter corresponds to the Gibbs free energies (ΔG°) of formation at the levels of theory labeled in the top row. The lowest energy ΔG° value for each method is denoted in bold.

formation of the $(H_2SO_4)_3$ clusters at room temperature calculated at M08-HX/MG3S//M08HX-MG3S, DLPNO-CCSD(T)-F12/cc-pVTZ-F12//M08-HX/MG3S, DLPNO-

CCSD(T)/CBS(Riemann)//M08-HX/MG3S, and DLPNO-CCSD(T)/CBS(4-5)//M08-HX/MG3S levels of theory, where CBS(Riemann) and CBS(4-5) correspond to three-point complete basis set limit extrapolations using the Riemann zeta function⁴⁹ and 4-5 inverse polynomial⁴⁸ extrapolation schemes along with aug-cc-pVnZ basis sets where n = D, T, Q. Tables S2–S6 in the Supporting Information present the ZPVE, ΔH° , and ΔG° values at 217, 273, and 298 K for all five methods discussed in this paper.

The minimum energy structures shift from T1 (Table 1) to T2 for the DFT method and from L2 (Table 1) to the linear Henschel structure once ΔG° is calculated at 298 K. The ΔG° formation values for DLPNO-CCSD(T)-F12/cc-pVTZ-F12 increase dramatically relative to the M08-HX/MG3S ΔG° values. In addition, moving from the F12 method to the Riemann and 4-5 CBS methods reveals that extrapolation to the CBS using the correlated double, triple, and quadruple basis sets result in another several kcal mol⁻¹ increase in Gibbs free energy. The Riemann and 4-5 CBS results are virtually identical relative to the expected error in this method of less than a kcal mol⁻¹.60-64 These differences in ΔG° will have a profound effect on efforts to calculate the initial growth of prenucleation complexes as ΔG° values are combined with concentrations of monomers in the atmosphere to predict the pathways for nucleation to occur. 1,10

CBS Enthalpies and Gibbs Free Energies as a Function of Temperature. Table 3 presents the DLPNO-CCSD(T)/CBS//M08-HX/MG3S ΔG° energies using the 4-5 extrapolation method for three temperatures that span the troposphere. Table 3 reveals that the linear structure L2 is the minimum at 217 K, while the Henschel structure is the minimum in Gibbs free energy at 273 and 298 K. The L2 minima are a bit more linear than the Henschel structure, with the S-S-S angle 11° straighter. There are many minima within a few kcal mol⁻¹ of the global minima at each temperature so that a Boltzmann distribution would need to be considered for the ensemble of structures that would be expected to be present at each temperature. Likewise, corrections to the ΔG values using scaled frequencies, or a

Table 3. DPLNO-CCSD(T)/CBS(4-5)//M08-HX/MG3S Thermodynamics of Formation of $(H_2SO_4)_3$ Clusters in Units of kcal mol⁻¹a

| | 216.65 K | | 273.15 K | | 298.15 K | |
|---------------|--------------------|--------------------|--------------------|--------------------|--------------------|--------------------|
| cluster | ΔH° | ΔG° | ΔH° | ΔG° | ΔH° | ΔG° |
| structure T1 | -29.56 | -10.58 | -29.50 | -5.63 | -29.45 | -3.45 |
| structure T2 | -30.57 | -12.47 | -30.44 | -7.77 | -30.36 | -5.69 |
| structure L1 | -30.72 | -12.56 | -30.61 | -7.84 | -30.54 | -5.75 |
| structure T3 | -28.44 | -9.97 | -28.34 | -5.17 | -28.27 | -3.04 |
| structure T4 | -29.20 | -11.28 | -29.07 | -6.63 | -28.99 | -4.58 |
| structure T5 | -29.33 | -11.08 | -29.21 | -6.34 | -29.14 | -4.25 |
| structure T6 | -29.18 | -10.95 | -29.07 | -6.21 | -29.00 | -4.12 |
| structure T7 | -29.88 | -11.96 | -29.77 | -7.30 | -29.70 | -5.24 |
| structure T8 | -29.57 | -11.86 | -29.40 | -7.26 | -29.32 | -5.23 |
| structure T9 | -30.50 | -12.84 | -30.41 | -8.25 | -30.35 | -6.22 |
| structure L2 | -31.01 | -13.98 | -30.89 | -9.56 | -30.82 | -7.61 |
| structure T10 | -30.16 | -12.58 | -30.05 | -8.01 | -29.98 | -6.00 |
| structure L3 | -30.68 | -13.81 | -30.56 | -9.42 | -30.49 | -7.49 |
| Henschel | -30.46 | -13.87 | -30.34 | -9.56 | -30.27 | -7.66 |
| Besel | -29.51 | -13.09 | -29.37 | -8.82 | -29.30 | -6.94 |

[&]quot;The first column lists the cluster names as presented in Figures 2 and 3. Then, each pair of columns thereafter corresponds to the enthalpy (ΔH°) and Gibbs free energies (ΔG°) of formation at the temperatures labeled in the top row. The global ΔG° minimum has been denoted in bold.

Table 4. Changes in the Thermodynamic Corrections (kcal mol^{-1}) Associated with the Formation of $(\mathrm{H_2SO_4})_3$ Structure T2 from Infinitely Separated Monomers Computed Using Unscaled (1.000) and Scaled (0.973) Harmonic Frequencies at the M08-HX/MG3S Level of Theory^a

| | 0 K | 216.65 K | | 273.15 K | | 298.15 K | |
|----------------|--------|----------|-----------|----------|--------|----------|--------|
| scaling factor | ZPE | Hcorr | Gcorr | Hcorr | Gcorr | Hcorr | Gcorr |
| 1.000 | 2.320 | -0.472 | 19.948 | -0.338 | 24.654 | -0.261 | 26.727 |
| 0.973 | 2.259 | -0.448 | 19.805 | -0.305 | 24.481 | -0.229 | 26.541 |
| Δ | -0.061 | 0.024 | -0.143 | 0.033 | -0.173 | 0.032 | -0.186 |
| arri 1.00 1 | .1 1 1 | | 1 1 1 . 1 | . (4) | | | |

^aThe difference between the scaled and unscaled values are listed in the last row (Δ) .

quasi-harmonic approximation, would be necessary to arrive at the most accurate ΔG° values. Yet, the differences between the F12 and CBS methods of extrapolation to arrive at ΔG° values for cluster formation is larger than these smaller corrections would provide.

Impact of Scaling Frequencies on Gibbs Free Energy of Formation. Scaling harmonic frequencies or calculating anharmonic frequencies is critical for spectroscopists who are trying to locate hydrogen-bonded molecular clusters in their experiments. 30,65,66 Yet, previous work has indicated that scaling has less impact on the resulting Gibbs free energy of formation values. 10,11,30 At the suggestion of a reviewer, we investigated this point by computing the effects of scaling frequencies on the thermodynamics of formation of structure T2, the DFT global minimum for Gibbs free energy. Truhlar and co-workers have shown that scaling M08-HX/MG3S harmonic frequencies by a factor of 0.973 yields accurate zeropoint vibrational energy (ZPE) values for a comprehensive database of molecules.⁶⁷ Table S11 in the Supporting Information lists the effects of no scaling (1.000) versus using Truhlar's scaling factor of 0.973 on the thermodynamic corrections computed for the bound (H₂SO₄)₃ structure T2, and Table S12 shows the same values for the H₂SO₄ monomer. Frequency scaling reduced the room temperature Gibbs free energy correction for the trimer by 2.34 kcal mol⁻¹ and for the monomer by 0.72 kcal mol⁻¹. Table 4 lists the changes in the thermodynamic corrections associated with the formation of structure T2 from infinitely separated monomers. The room temperature Gibbs free energy correction changes by only 0.186 kcal mol⁻¹, suggesting that scaling harmonic frequencies results in negligible changes in the thermodynamic corrections used in computing Gibbs free energies of formation.

CONCLUSIONS

We have presented the electronic energies and thermodynamic corrections for the formation of the sulfuric acid trimer computed at various levels of theory. Specifically, the method of correcting DFT electronic contributions with DLPNO-CCSD(T) and its explicitly correlated counterpart was examined within the context of the final Gibbs free energies of formation. We found that the DLPNO-CCSD(T) methods always return more positive electronic energies compared to the DFT energy corresponding to the optimized geometries. Therefore, the final Gibbs free energies computed using DFT vibrational frequencies along with high-level electronic energies are always more positive compared to the pure DFT free energies. Within the DLPNO-CCSD(T) methods, we have shown that extrapolating to the complete basis set limit gives even more positive free energies when compared to explicitly correlated single-point energies. The CBS extrapolation was shown to be robust since both the 4-5 inverse polynomial and

Riemann zeta function schemes were well within chemical accuracy of one another. Furthermore, we note that the first PM7 step of configurational sampling in the GA/DFT/DLPNO funnel methodology must retain as many structures as possible for the subsequent DFT geometry optimizations due to the risk of missing important local minima that can eventually converge to the ensemble of DFT global minima.

ASSOCIATED CONTENT

5 Supporting Information

The Supporting Information is available free of charge at https://pubs.acs.org/doi/10.1021/acs.jpca.1c00872.

The nomenclature that relates the names assigned in the paper to the names assigned by the genetic algorithm (Table S1); M08-HX/MG3S energies (Table S2); DLPNO-CCSD(T)-F12/cc-pVTZ-F12 energies (Table S3); DLPNO-CCSD(T)/4-5 polynomial CBS extrapolation energies (Table S4); DLPNO-CCSD(T)/ Riemann zeta CBS extrapolation energies (Table S5); DLPNO-CCSD(T)-F12/cc-pVQZ-F12 energies (Table S6); M08-HX/MG3S thermal corrections (Table S7); M08-HX/MG3S and DLPNO-CCSD(T)-F12/ccpVnZ-F12 (n = T, Q) absolute electronic energies (Table S8); DLPNO-CCSD(T)/aug-cc-pVnZ (n = D, T, and Q) absolute electronic energies (Table S9); DLPNO-CCSD(T)/CBS absolute electronic energies (Table S10); structure T2 thermodynamic corrections computed with unscaled and scaled harmonic frequencies (Table S11); sulfuric acid thermodynamic corrections computed with unscaled and scaled harmonic frequencies (Table S12); energy distributions of structure T2 at PM7, M08-HX/6-31+G*, and M08-HX/MG3S levels of theory (Figure S1); optimized geometries at the M08-HX/MG3S level of theory (Section 3); and derivation of complete basis set limit extrapolation formulas (Section 4) (PDF)

AUTHOR INFORMATION

Corresponding Author

George C. Shields — Department of Chemistry, Furman University, Greenville, South Carolina 29613-0002, United States; orcid.org/0000-0003-1287-8585; Email: George.shields@furman.edu

Authors

Luke A. Kurfman – Department of Chemistry, Furman University, Greenville, South Carolina 29613-0002, United States

Tuguldur T. Odbadrakh – Department of Chemistry, Furman University, Greenville, South Carolina 29613-0002, United States

Complete contact information is available at: https://pubs.acs.org/10.1021/acs.jpca.1c00872

Notes

The authors declare no competing financial interest.

ACKNOWLEDGMENTS

Funding for this work was provided by grants CHE-1229354, CHE 1662030, CHE-1903871, and CHE-2018427 from the National Science Foundation (GCS). High-performance computing resources were provided by the MERCURY Consortium (www.mercuryconsortium.org).⁶⁸

REFERENCES

- (1) Leonardi, A.; Ricker, H. M.; Gale, A. G.; Ball, B. T.; Odbadrakh, T. T.; Shields, G. C.; Navea, J. G. Particle formation and surface processes on atmospheric aerosols: A review of applied quantum chemical calculations. *Int. J. Quantum Chem.* **2020**, *120*, No. e26350.
- (2) Sipila, M.; Berndt, T.; Petaja, T.; Brus, D.; Vanhanen, J.; Stratmann, F.; Patokoski, J.; Mauldin, R. L.; Hyvarinen, A. P.; Lihavainen, H.; Kulmala, M. The role of sulfuric acid in atmospheric nucleation. *Science* **2010**, *327*, 1243–1246.
- (3) Boucher, O.; Lohmann, U. The sulfate-CCN-cloud albedo effect. *Tellus, Ser. B: Chem. Phys. Meteorol.* **2017**, 47, 281–300.
- (4) Seinfeld, J. H.; Pandis, S. N., Atmospheric Chemistry and Physics: From Air Pollution to Climate Change; 2 ed.; John Wiley & Sons, Inc.: New York. 2006.
- (5) Alongi, K. S.; Dibble, T. S.; Shields, G. C.; Kirschner, K. N. Exploration of the potential energy surfaces, prediction of atmospheric concentrations, and prediction of vibrational spectra for the HO_2 ... $(H_2O)_n$ (n = 1-2) hydrogen bonded complexes. *J. Phys. Chem. A* **2006**, *110*, 3686–3691.
- (6) Allodi, M. A.; Dunn, M. E.; Livada, J.; Kirschner, K. N.; Shields, G. C. Do hydroxyl radical-water clusters, OH(H₂O)_n, n = 1-5, exist in the atmosphere? *J. Phys. Chem. A* **2006**, *110*, 13283–13289.
- (7) Kirschner, K. N.; Shields, G. C. Quantum-Mechanical Investigation of Large Water Clusters. *Int. J. Quantum Chem.* **1994**, 52, 349–360.
- (8) Shields, G. C.; Kirschner, K. N. The limitations of certain density functionals in modeling neutral water clusters. *Synth. React. Inorg., Met.-Org., Nano-Met. Chem.* **2008**, 38, 32–39.
- (9) Pickard, F. C., IV; Pokon, E. K.; Liptak, M. D.; Shields, G. C. Comparison of CBS-QB3, CBS-APNO, G2, and G3 thermochemical predictions with experiment for formation of ionic clusters of hydronium and hydroxide ions complexed with water. *J. Chem. Phys.* **2005**, *122*, No. 024302.
- (10) Temelso, B.; Morrell, T. E.; Shields, R. M.; Allodi, M. A.; Wood, E. K.; Kirschner, K. N.; Castonguay, T. C.; Archer, K. A.; Shields, G. C. Quantum mechanical study of sulfuric acid hydration: atmospheric implications. *J. Phys. Chem. A* **2012**, *116*, 2209–2224.
- (11) Temelso, B.; Phan, T. N.; Shields, G. C. Computational study of the hydration of sulfuric acid dimers: implications for acid dissociation and aerosol formation. *J. Phys. Chem. A* **2012**, *116*, 9745–9758
- (12) Pickard, F. C.; Dunn, M. E.; Shields, G. C. Comparison of model chemistry and density functional theory thermochemical predictions with experiment for formation of ionic clusters of the ammonium cation complexed with water and ammonia; atmospheric implications. J. Phys. Chem. A 2005, 109, 4905–4910.
- (13) Temelso, B.; Morrison, E. F.; Speer, D. L.; Cao, B. C.; Appiah-Padi, N.; Kim, G.; Shields, G. C. Effect of Mixing Ammonia and Alkylamines on Sulfate Aerosol Formation. *J. Phys. Chem. A* **2018**, 122, 1612–1622.
- (14) Hartt, G. M.; Shields, G. C.; Kirschner, K. N. Hydration of OCS with one to four water molecules in atmospheric and laboratory conditions. *J. Phys. Chem. A* **2008**, *112*, 4490–4495.

- (15) Husar, D. E.; Temelso, B.; Ashworth, A. L.; Shields, G. C. Hydration of the bisulfate ion: atmospheric implications. *J. Phys. Chem. A* **2012**, *116*, 5151–5163.
- (16) Morrell, T. E.; Shields, G. C. Atmospheric implications for formation of clusters of ammonium and 1-10 water molecules. *J. Phys. Chem. A* **2010**, *114*, 4266–4271.
- (17) Perdew, J. P.; Burke, K.; Ernzerhof, M. Generalized gradient approximation made simple. *Phys. Rev. Lett.* **1997**, *78*, 1396–1396.
- (18) Becke, A. D. Density-functional thermochemistry. III. The role of exact exchange. *J. Chem. Phys.* **1993**, *98*, 5648–5652.
- (19) Chai, J. D.; Head-Gordon, M. Systematic optimization of long-range corrected hybrid density functionals. *J. Chem. Phys.* **2008**, *128*, No. 084106.
- (20) Ditchfield, R.; Hehre, W. J.; Pople, J. A. Self-consistent molecular-orbital methods. IX. An extended Gaussian-type basis for molecular-orbital studies of organic molecules. *J. Chem. Phys.* **1971**, 54, 724–728.
- (21) Neese, F.; Hansen, A.; Liakos, D. G. Efficient and accurate approximations to the local coupled cluster singles doubles method using a truncated pair natural orbital basis. *J. Chem. Phys.* **2009**, *131*, No. 064103.
- (22) Neese, F.; Hansen, A.; Wennmohs, F.; Grimme, S. Accurate theoretical chemistry with coupled pair models. *Acc. Chem. Res.* **2009**, 42, 641–648.
- (23) Neese, F.; Wennmohs, F.; Hansen, A. Efficient and accurate local approximations to coupled-electron pair approaches: An attempt to revive the pair natural orbital method. *J. Chem. Phys.* **2009**, *130*, 114108.
- (24) Hansen, A.; Liakos, D. G.; Neese, F. Efficient and accurate local single reference correlation methods for high-spin open-shell molecules using pair natural orbitals. *J. Chem. Phys.* **2011**, *135*, 214102
- (25) Riplinger, C.; Neese, F. An efficient and near linear scaling pair natural orbital based local coupled cluster method. *J. Chem. Phys.* **2013**, *138*, No. 034106.
- (26) Riplinger, C.; Sandhoefer, B.; Hansen, A.; Neese, F. Natural triple excitations in local coupled cluster calculations with pair natural orbitals. *J. Chem. Phys.* **2013**, *139*, 134101.
- (27) Liakos, D. G.; Sparta, M.; Kesharwani, M. K.; Martin, J. M. L.; Neese, F. Exploring the accuracy limits of local pair natural orbital coupled-cluster theory. *J. Chem. Theory Comput.* **2015**, *11*, 1525–1539.
- (28) Liakos, D. G.; Neese, F. Is it possible to obtain coupled cluster quality energies at near density functional theory cost? Domain-based local pair natural orbital coupled cluster vs modern density functional theory. *J. Chem. Theory Comput.* **2015**, *11*, 4054–4063.
- (29) Guo, Y.; Riplinger, C.; Becker, U.; Liakos, D. G.; Minenkov, Y.; Cavallo, L.; Neese, F. Communication: An improved linear scaling perturbative triples correction for the domain based local pair-natural orbital based singles and doubles coupled cluster method [DLPNO-CCSD(T)]. J. Chem. Phys. 2018, 148, No. 011101.
- (30) Dunn, M. E.; Evans, T. M.; Kirschner, K. N.; Shields, G. C. Prediction of accurate anharmonic experimental vibrational frequencies for water clusters, (H2O)n, n=2-5. *J. Phys. Chem. A* **2006**, *110*, 303–309.
- (31) Myllys, N.; Elm, J.; Kurtén, T. Density functional theory basis set convergence of sulfuric acid-containing molecular clusters. *Computational and Theoretical Chemistry* **2016**, *1098*, 1–12.
- (32) Dieterich, J. M.; Hartke, B. OGOLEM: Global cluster structure optimisation for arbitrary mixtures of flexible molecules. A multiscaling, object-oriented approach. *Mol. Phys.* **2010**, *108*, 279–291.
- (33) Hostaš, J.; Řezáč, J.; Hobza, P. On the performance of the semiempirical quantum mechanical PM6 and PM7 methods for noncovalent interactions. *Chem. Phys. Lett.* **2013**, 568-569, 161–166.
- (34) Stewart, J. J. P. *MOPAC2016*, Stewart Computational Chemistry: Colorado Springs, CO, USA, 2016.
- (35) Zhao, Y.; Truhlar, D. G. Exploring the limit of accuracy of the global hybrid meta density functional for main-group thermochem-

- istry, kinetics, and noncovalent interactions. *J. Chem. Theory Comput.* **2008**, *4*, 1849–1868.
- (36) Krishnan, R.; Binkley, J. S.; Seeger, R.; Pople, J. A. Self-consistent molecular orbital methods. XX. A basis set for correlated wave functions. *J. Chem. Phys.* **1980**, *72*, 650–654.
- (37) Frisch, M. J.; Trucks, G. W.; Schlegel, H. B.; Scuseria, G. E.; Robb, M. A.; Cheeseman, J. R.; Scalmani, G.; Barone, V.; Petersson, G. A.; Nakatsuji, H. *Gaussian 16 Rev. B.01*, Wallingford, CT, 2016.
- (38) Clark, T.; Chandrasekhar, J.; Spitznagel, G. W.; Schleyer, P. V. R. Efficient diffuse function-augmented basis sets for anion calculations. III. The 3-21+G basis set for first-row elements, Li-F. *J. Comput. Chem.* 1983, 4, 294–301.
- (39) Frisch, M. J.; Pople, J. A.; Binkley, J. S. Self-consistent molecular orbital methods 25. Supplementary functions for Gaussian basis sets. *J. Chem. Phys.* **1984**, *80*, 3265–3269.
- (40) Irikura, K. K. In Computational thermochemistry: Prediction and estimation of molecular thermodynamics, ACS Symposium Series, Irikura, K. K.; Frurip, D. J., Eds. American Chemical Society: 1998, DOI: 10.1021/bk-1998-0677.
- (41) Irikura, K. K. *THERMO.PL*, National Institute of Standards and Technology: 2002.
- (42) Odbadrakh, T. T.; Gale, A. G.; Ball, B. T.; Temelso, B.; Shields, G. C. Computation of atmospheric concentrations of molecular clusters from ab initio thermochemistry. *J. Visualized Exp.* **2020**, 158.
- (43) Liakos, D. G.; Izsák, R.; Valeev, E. F.; Neese, F. What is the most efficient way to reach the canonical MP2 basis set limit? *Mol. Phys.* **2013**, *111*, 2653–2662.
- (44) Riplinger, C.; Pinski, P.; Becker, U.; Valeev, E. F.; Neese, F. SparseMaps—A systematic infrastructure for reduced-scaling electronic structure methods. II. Linear scaling domain based pair natural orbital coupled cluster theory. *J. Chem. Phys.* **2016**, *144*, No. 024109.
- (45) Pavosevic, F.; Pinski, P.; Riplinger, C.; Neese, F.; Valeev, E. F. SparseMaps–A systematic infrastructure for reduced-scaling electronic structure methods. IV. Linear-scaling second-order explicitly correlated energy with pair natural orbitals. *J. Chem. Phys.* **2016**, *144*, 144109.
- (46) Neese, F. The ORCA program system. *WIREs Comput. Mol. Sci.* **2011**, *2*, 73–78.
- (47) Neese, F. Software update: the ORCA program system, version 4.0. WIREs Comput. Mol. Sci. 2017, 8, e127.
- (48) Helgaker, T.; Klopper, W.; Koch, H.; Noga, J. Basis-set convergence of correlated calculations on water. *J. Chem. Phys.* **1997**, 106, 9639–9646.
- (49) Lesiuk, M.; Jeziorski, B. Complete basis set extrapolation of electronic correlation energies using the Riemann zeta function. *J. Chem. Theory Comput.* **2019**, *15*, 5398–5403.
- (50) Yousaf, K. E.; Peterson, K. A. Optimized complementary auxiliary basis sets for explicitly correlated methods: aug-cc-pVnZ orbital basis sets. *Chem. Phys. Lett.* **2009**, *476*, 303–307.
- (51) Herb, J.; Nadykto, A. B.; Yu, F. Large ternary hydrogen-bonded pre-nucleation clusters in the Earth's atmosphere. *Chem. Phys. Lett.* **2011**, *518*, 7–14.
- (52) Kubecka, J.; Besel, V.; Kurten, T.; Myllys, N.; Vehkamaki, H. Configurational sampling of noncovalent (atmospheric) molecular clusters: Sulfuric acid and guanidine. *J. Phys. Chem. A* **2019**, *123*, 6022–6033.
- (53) de Souza Gonçalves, D.; Chaudhuri, P. Atmospherically relevant hydrogen-bonded interactions between methanesulfonic acid and H2SO4 clusters: A computational study. *J. Phys. Chem. A* **2020**, *124*, 11072–11085.
- (54) Pettersen, E. F.; Goddard, T. D.; Huang, C. C.; Couch, G. S.; Greenblatt, D. M.; Meng, E. C.; Ferrin, T. E. UCSF Chimera–a visualization system for exploratory research and analysis. *J. Comput. Chem.* **2004**, *25*, 1605–1612.
- (55) Jurema, M. W.; Shields, G. C. Ability of the PM3 quantum-mechanical method to modelintermolecular hydrogen bonding between neutral molecules. *J. Comput. Chem.* **1993**, *14*, 89–104.
- (56) Henschel, H.; Navarro, J. C. A.; Yli-Juuti, T.; Kupiainen-Maatta, O.; Olenius, T.; Ortega, I. K.; Clegg, S. L.; Kurten, T.; Riipinen, I.;

- Vehkamaki, H. Hydration of atmospherically relevant molecular clusters: computational chemistry and classical thermodynamics. *J. Phys. Chem. A* **2014**, *118*, 2599–2611.
- (57) Torpo, L.; Kurten, T.; Vehkamaki, H.; Laasonen, K.; Sundberg, M. R.; Kulmala, M. Significance of ammonia in growth of atmospheric nanoclusters. *J. Phys. Chem. A* **2007**, *111*, 10671–10674.
- (58) Besel, V.; Kubecka, J.; Kurten, T.; Vehkamaki, H. Impact of quantum chemistry parameter choices and cluster distribution model settings on model atmospheric particle formation rates. *J. Phys. Chem.* A **2020**, *124*, 5931–5943.
- (59) Temelso, B.; Mabey, J. M.; Kubota, T.; Appiah-Padi, N.; Shields, G. C. ArbAlign: A Tool for Optimal Alignment of Arbitrarily Ordered Isomers Using the Kuhn-Munkres Algorithm. *J. Chem. Inf. Model.* **2017**, *57*, 1045–1054.
- (60) Howard, J. C.; Gray, J. L.; Hardwick, A. J.; Nguyen, L. T.; Tschumper, G. S. Getting down to the fundamentals of hydrogen bonding: Anharmonic vibrational frequencies of (HF)2 and (H2O)2 from ab initio electronic structure computations. *J. Chem. Theory Comput.* **2014**, *10*, 5426–5435.
- (61) Temelso, B.; Renner, C. R.; Shields, G. C. Importance and reliability of small basis set CCSD(T) corrections to MP2 binding and relative rnergies of water clusters. *J. Chem. Theory Comput.* **2015**, *11*, 1439–1448.
- (62) Johnson, S. N.; Tschumper, G. S. Hydrogen bonding in the mixed HF/HCl dimer: Is it better to give or receive? *J. Comput. Chem.* **2018**, *39*, 839–843.
- (63) Sexton, T. M.; Howard, J. C.; Tschumper, G. S. Dissociation energy of the H2O...HF dimer. *J. Phys. Chem. A* **2018**, *122*, 4902–4908.
- (64) Schwan, R.; Qu, C.; Mani, D.; Pal, N.; Schwaab, G.; Bowman, J. M.; Tschumper, G. S.; Havenith, M. Observation of the low-frequency spectrum of the water trimer as a sensitive test of the water-trimer potential and the dipole-moment surface. *Angew. Chem., Int. Ed.* **2020**, 59, 11399–11407.
- (65) Kreinbihl, J. J.; Frederiks, N. C.; Waller, S. E.; Yang, Y.; Johnson, C. J. Establishing the structural motifs present in small ammonium and aminium bisulfate clusters of relevance to atmospheric new particle formation. *J. Chem. Phys.* **2020**, *153*, No. 034307.
- (66) Knorke, H.; Li, H.; Liu, Z. F.; Asmis, K. R. Vibrational spectroscopy of the hexahydrated sulfate dianion revisited: role of isomers and anharmonicities. *Phys. Chem. Chem. Phys.* **2019**, 21, 11651–11659.
- (67) Alecu, I. M.; Zheng, J.; Zhao, Y.; Truhlar, D. G. Computational thermochemistry: Scale factor databases and scale factors for vibrational frequencies obtained from electronic model chemistries. *J. Chem. Theory Comput.* **2010**, *6*, 2872–2887.
- (68) Shields, G. C. Twenty years of exceptional success: The molecular education and research consortium in undergraduate computational chemistry (MERCURY). *Int. J. Quantum Chem.* **2020**, *120*, No. e26274.